Progress In Electromagnetics Research C, Vol. 61, 149–159, 2016

Compact WLAN Band-notched Printed Ultrawideband MIMO Antenna with Polarization Diversity

Beegum S. Femina and Sanjeev K. Mishra*

Abstract—A novel uniplanar compact WLAN band-notched printed ultra wideband (UWB) multiple-input multiple-output (MIMO) antenna with dual polarization for high data-rate wireless communication is proposed. The antenna consists of two CPW-fed floral radiating elements along with a decoupling structure to ensure high isolation. The band notch at the WLAN frequency band is achieved by etching one single U-shaped slot on each antenna element. Results show that the proposed antenna gives impedance bandwidth from 2.7 GHz to 10.9 GHz with notched frequency band from 5.1 GHz to 5.9 GHz. The proposed antenna provides nearly omnidirectional radiation pattern, low envelope correction coefficient [ECC], moderate gain, efficiency, fidelity factor and pattern stability factor [PSF]. Furthermore, diversity characteristics such as mean effective gain [MEG] and diversity gain [DG] are also studied. Moreover, the time-domain analysis displays minimum dispersion to the radiated pulse. All these features make the proposed antenna a good candidate for future high data-rate wireless communication systems with polarization-diversity operation, where the challenge of multipath fading is a major concern.

1. INTRODUCTION

Recently, the combination of ultra wideband technology with multiple-input multiple-output (MIMO), owing to its large bandwidth and high data transmission, has attracted significant research attention for its well-known advantages of reducing the multipath fading and increasing transmission capacity [1, 2]. However, in wireless communication, multipath due to reflection and diffraction is a major concern when the signals with different amplitudes and phases combine destructively at the receiver. Multipath fading can be solved by diversity technology such as spatial diversity, time diversity, pattern diversity, and polarization diversity. The polarization diversity is one of the very effective techniques to mitigate fading which helps to increase channel capacity, transmission quality and greatly improves the spectrum efficiency [2–4].

As key components of UWB systems, wideband and high-isolation characteristics are required for UWB diversity antennas, which have been studied widely in recent years, in particular etching a ring slot on the ground plane [5], extending a tree-like structure [6] and inserting stubs [7] between the two radiating elements to weaken the mutual coupling. Parasitic elements were also inserted between the elements to improve the isolation at a given frequency [8]. Decoupling can also be achieved by inserting a neutralization line into antenna elements [9]. Dual polarization is another efficient method to realize decoupling and enhance reliability in the wireless communication system [10–12]. At the same time, although the Federal Communications Commission (FCC) allowed commercial use of the UWB band of 3.1–10.6 GHz, there are other narrowband communication systems, such as the IEEE 802.11 wireless local area network (WLAN) centred at 5.5 GHz, which may cause possible electromagnetic interference to the UWB applications. To avoid this, many significant band-notched techniques have

Received 11 November 2015, Accepted 5 January 2016, Scheduled 16 January 2016
* Corresponding author: Sanjeev Kumar Mishra (sanjeevkmishra@iist.ac.in).
The authors are with the Department of Avionics, Indian Institute of Space Sapience and Technology (IIST), Trivandrum-695547, India.

been proposed for UWB antennas, including inserting inverted T-shaped strips protruding inside the square-ring radiating patch [13], electromagnetic band-gap (EBG) structures [14], split-ring resonator (SRR) structures, microstrip open-loop resonator and configuring p-i-n diodes [15, 16].

In this paper, a new compact, uniplanar, UWB dual-polarized antenna embedded with WLAN band reject filter for MIMO applications is proposed. The proposed antenna consists of two identical band notched floral monopole antennas (BNFMPA) fed by coplanar waveguides, which are designed to achieve UWB orthogonal polarizations. A rectangular isolation stub is placed at 45° between the two radiators to ensure isolations. The coplanar waveguide (CPW) feed provides advantages such as low dispersion, low radiation loss and easy integration with monolithic microwave integrated circuits. Results, i.e., impedance bandwidth, gain, group delay, transfer function, fidelity factor, PSF, ECC, MEG, and DG are analysed and reported in following sections.

2. ANTENNA GEOMETRY AND DESIGN

Figure 1 shows the geometry of the proposed UWB-MIMO antenna of size $50 \times 45 \times 0.787\,\text{mm}^3$ along with its evolution. The basic antenna structure, which consists of two identical floral radiating antenna

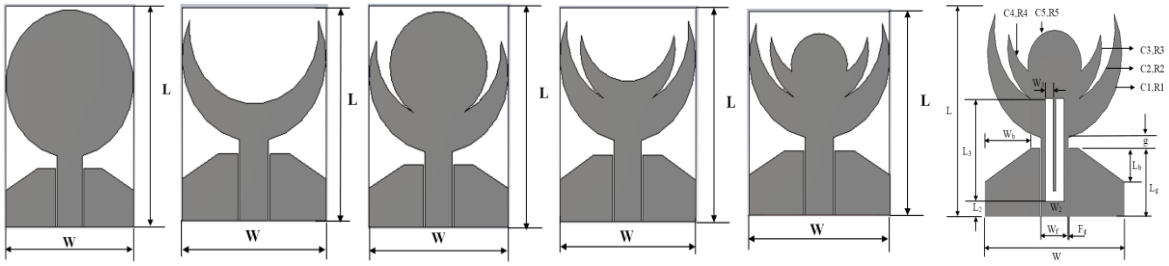

(a)

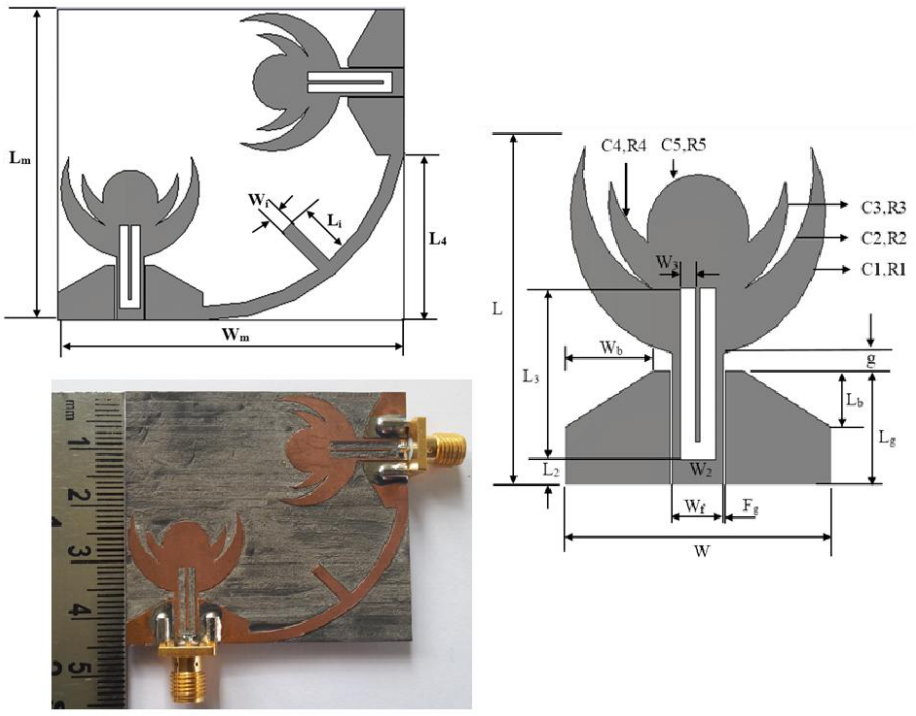

(b)

Figure 1. (a) Evolution of floral monopole antenna, (b) geometry and photograph of proposed UWB-MIMO antenna.

elements, is orthogonally excited through coplanar waveguide feed lines. The evolution of basic floral shape structure as shown in Figure 1(a) is a variation of circular monopole antenna.

The radius (R) of circular monopole [10] is obtained by using the following equation

$$f_L = \frac{7.2}{2.25R + g}\,\text{GHz} \tag{1}$$

where g is the gap between radiating patch and ground plane and f_L the lowest resonant frequency corresponding to VSWR = 2.

Further antenna design is based on the fact that the current is mainly concentrated along the lower periphery of the circular monopole antenna. So, the upper and central portions can be removed with negligible effect on impedance bandwidth and radiation characteristics, resulting in crescent moon structure. Similarly, smaller circular areas are added and removed to result in a lotus-shaped floral monopole antenna that minimizes the distortion of radiation pattern in the upper frequencies of UWB band. The structure is optimized such that $S_{11} \leq -10\,\text{dB}$ over the UWB frequency range. The ground planes are beveled, which results in a smooth transition from one resonant mode to another and ensures good impedance match over a broad frequency range. Thereafter, band-notched characteristic is obtained by etching a U-shaped slot in the radiating structure, which has negligible effect at other frequencies in UWB. The dimensions of half-wave resonating slot at central band-notched frequency can be postulated as

$$f_{\text{notch}} = \frac{c}{2L_S\sqrt{\varepsilon_{eff}}} \tag{2}$$

where $L_S = [2L_3 + W_2]$ is the total length, W_3 the width of the U-shaped slot, ε_{eff} the effective dielectric constant and c the speed of the light.

The two identical floral radiating antenna elements, as shown in Figure 1(b), are orthogonally excited through coplanar waveguide feed lines, and a simple stub is introduced in the ground plane to enhance the inter port isolation. The antenna structure is printed on a Rogers RT/Duroid 5880 with permittivity (ε_r) 2.2, loss tangent 0.0012 and thickness (h) 0.787 mm. The optimized dimensions as per Table 1 provide good impedance matching leading to desired frequency band. The merging of several dominant resonances provides a broad impedance bandwidth as shown in Figure 2.

Table 1. Design parameters of BNFMPA MIMO.

Parameter	$C1$, $R1$	$C3$, $R3$	$C5$, $R5$		L_2	h	W_2
Dimensions (mm)	(x: 10, y: 19.50), 10	(x: 10, y: 20.75), 7	(x: 10, y: 18.75), 4		3	0.787	2.8
Parameter	$C2$, $R2$	$C4$, $R4$	W	L	L_3	t	W_3
Dimensions (mm)	(x: 10, y: 21.50), 9	(x: 10, y: 23.75), 7	21	24.5	12	0.035	1.2
Parameter	L_b	W_f	F_g	L_4	L_i	L_m	-
Dimensions (mm)	4	4	0.2	24	7.5	45	-
Parameter	W_b	g	L_g	W_i		W_m	-
Dimensions (mm)	7	2	8	2		50	-

The antenna shows a desired notch in the IEEE 802.11a and HIPERLAN/2 bands, when the length of the slot resonator is approximately a half-wavelength long at the center notch frequency. The initial analysis and optimization of the antenna were performed using CST Microwave Studio, and measurements were carried out with an Agilent N5224A vector network analyzer. The reflection parameter of the proposed antenna element is measured through one of the ports while the other port is terminated with 50 Ω load.

3. RESULTS AND DISCUSSION

The measured and simulated S-parameters of the proposed antenna at port-1 and port-2 are presented in Figure 2. Due to the geometrical symmetry, the simulated results for both ports are identical. The antenna displays impedance bandwidth from 2.7 to 10.9 GHz with inter-port isolation better than

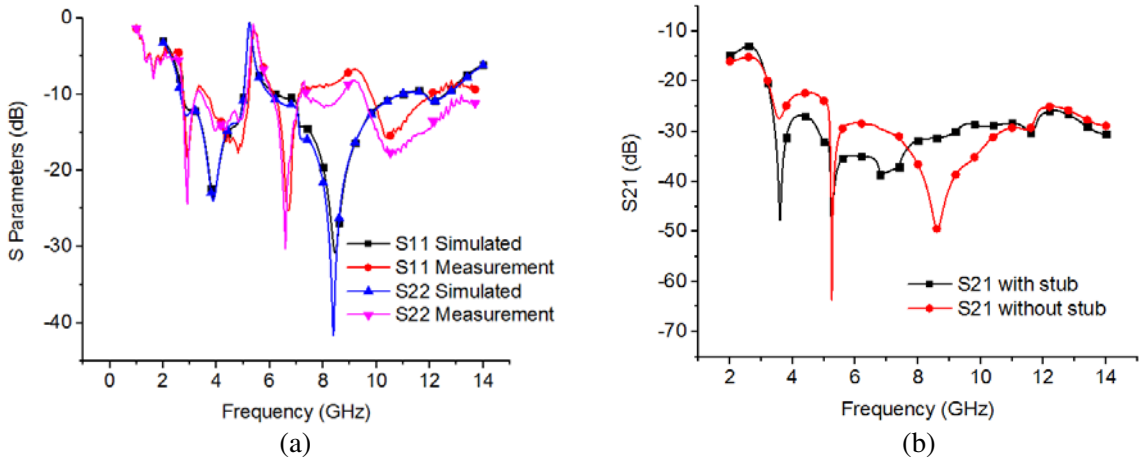

Figure 2. (a) Simulated and measured S parameters of the proposed antenna and (b) transmission coefficient with and without stub.

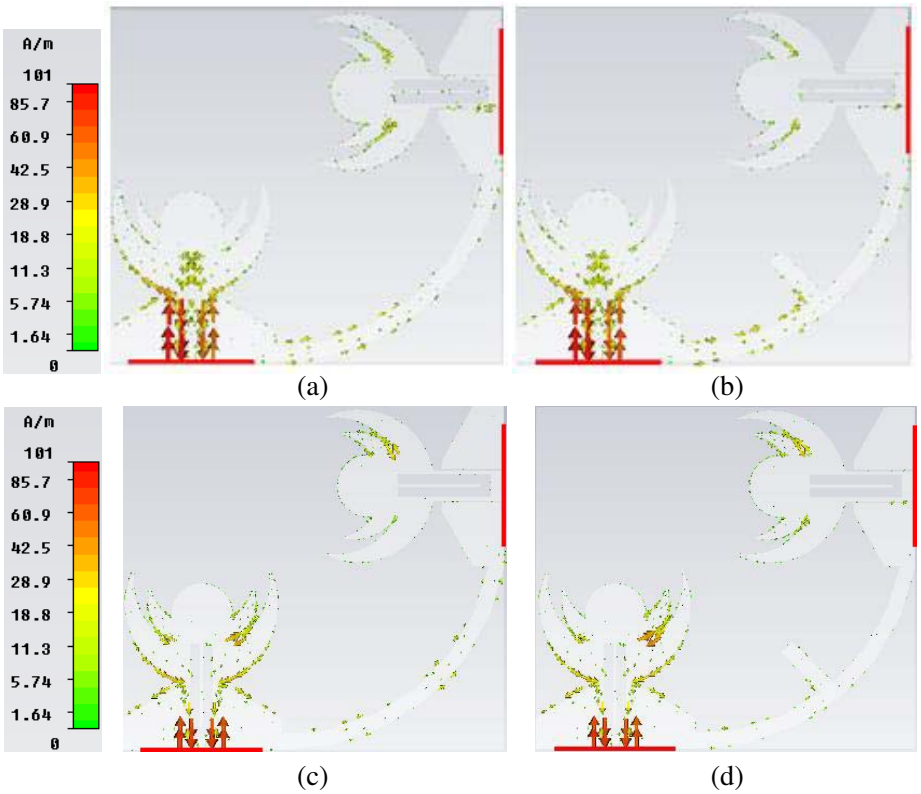

Figure 3. Magnitude of surface current distribution (a) at 4 GHz without isolation stub, (b) at 4 GHz with isolation stub, (c) at 10 GHz without isolation stub and (d) at 10 GHz with isolation stub.

−25 dB throughout the desired frequency band. It also provides a notch frequency band from 5.1 to 5.9 GHz. The slight differences between the measured and simulated scattering parameters are due to soldering, fabrication tolerances and presence of connector. Moreover, the RF cables from the vector network analyzer have influence on the measurements of small antennas [13]. It is observed that various types of isolation strips provide isolation better than 15 dB at the lower frequency region of the spectrum. However, only a simple stub with proposed configuration enhances the isolation better than 25 dB. The

influence of a simple stub on radiation pattern compared to the basic antenna was also analyzed and found minimal.

Surface current distribution of the proposed antenna is analyzed to further investigate the effect of the decoupling structure. The magnitudes of the surface current density at 4 and 10 GHz are illustrated in Figures 3(a)–(d), which aids better understanding about the isolation mechanism of the antenna. It is observed that when port 1 is excited without the isolation stub, the current from port 1 has a high tendency to couple the port 2 through the common ground plane. However, the integration of the isolation stub reduces the current on the ground plane around port 2 when port 1 is excited (vice versa when port 2 is excited). This is due to the strong current excitation on the stub, which results in better inter-port isolation and thereby significantly improves the diversity performance.

The far-field (2-D) radiation patterns of the proposed antenna at 3 GHz and 10 GHz are shown in Figure 4 assuming that antenna is oriented in XY plane. The independent pattern on each port (port 2 is connected to the matched load when port 1 is excited, and vice versa) exhibits quasi-omnidirectional radiation patterns. It is worth to note that the patterns at port 1 and port 2 are similar with a 90° rotation, which in turn confirms dual polarization. Figure 5 shows the antenna gain over the desired frequency band of the proposed antenna. It is observed that the antenna keeps a stable gain about 2 dBi over the UWB frequency band except WLAN frequency band of 5.1 to 5.9 GHz. The simulated radiation efficiency, namely the ratio of total radiated power to net power accepted by the antenna at its terminals, is depicted in Figure 6. It is observed that the antenna provides efficiency better than 75% in the UWB spectrum, while there is a sharp decrease in the notch frequency band.

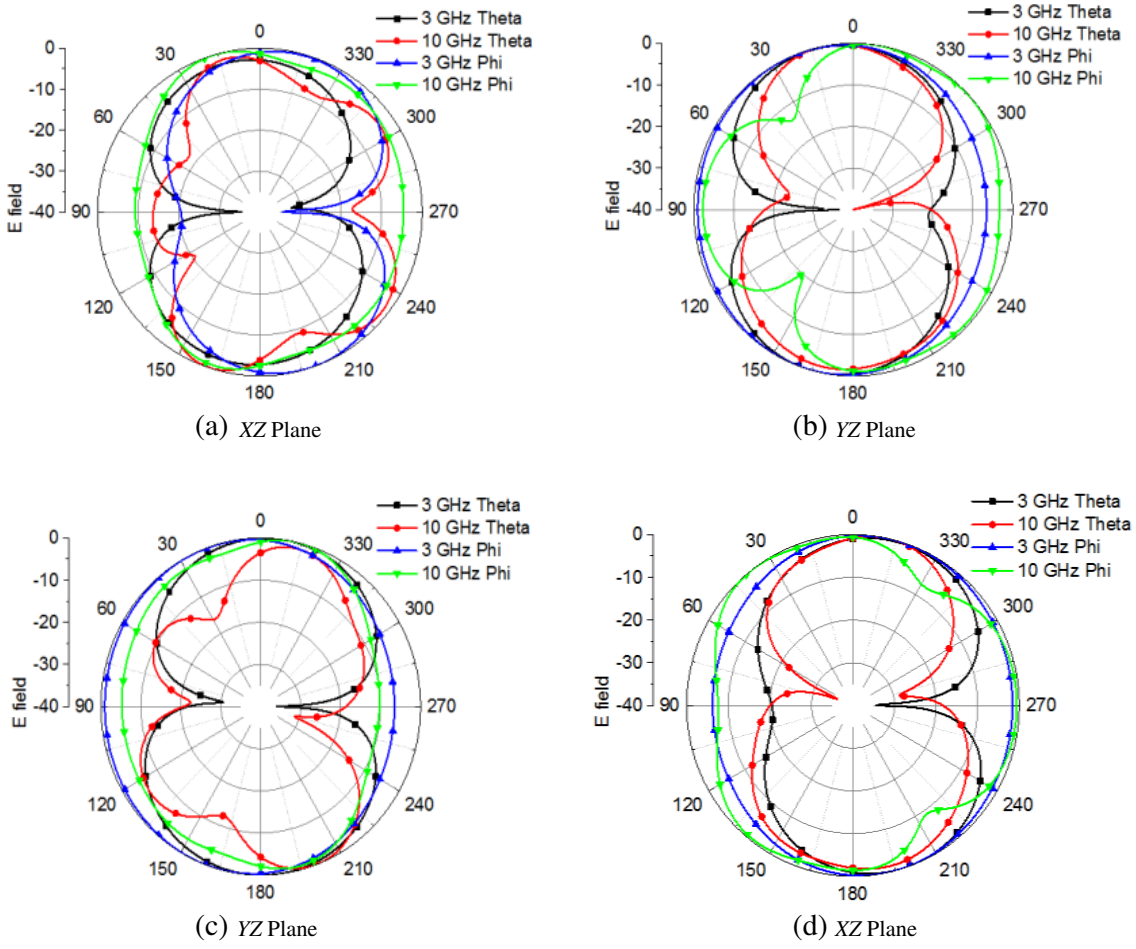

Figure 4. Radiation patterns (theta and phi components of E field) of proposed antenna (a), (b) port 1 excited, (c) and (d) port 2 excited.

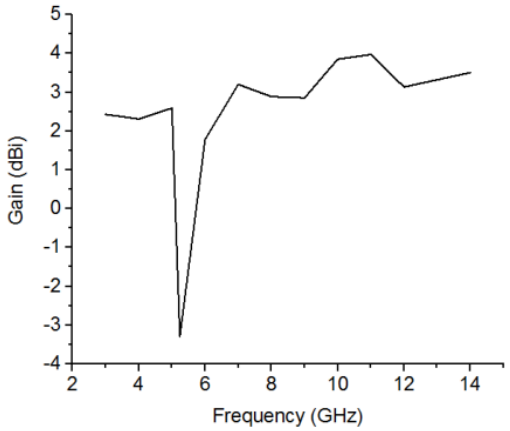

Figure 5. Gain of proposed antenna.

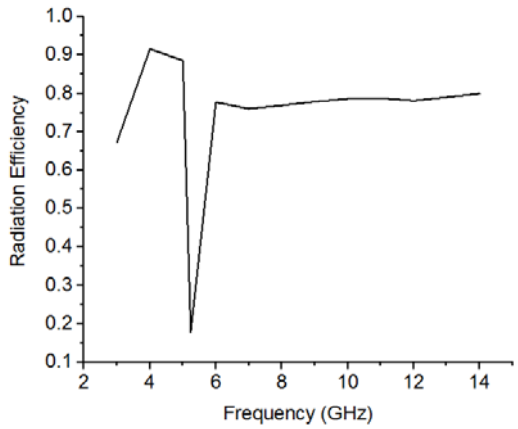

Figure 6. Radiation efficiency of proposed antenna.

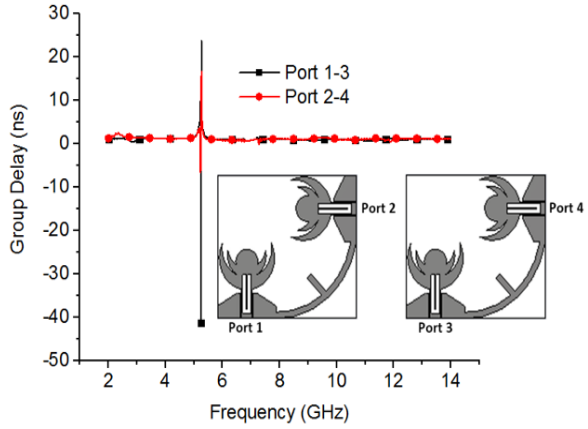

(a)

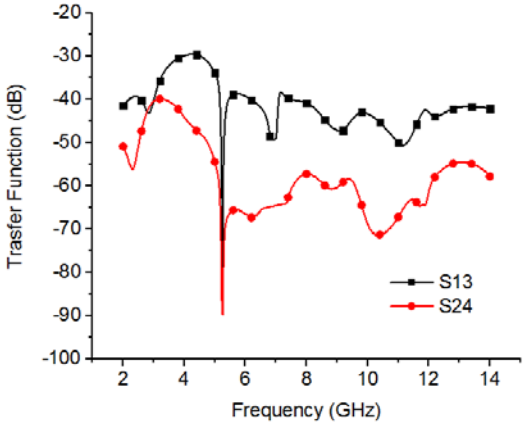

(b)

Figure 7. (a) Group delay and (b) antenna transfer function [$R = 250$ mm].

In a UWB system, the antenna needs to possess a high level of pulse-handling capability to handle high-frequency impulses. Hence, the time-domain properties are equally as important as frequency domain. The group delay, transfer function, fidelity factor, etc. of the proposed structure are obtained by placing two identical antennas in the far field, and their port definitions for desired configuration are shown in Figure 7(a). The group delay of the antenna, measured in the far field with end-to-end orientation (when port 1 is excited and port 2 terminated with 50 Ω load and vice versa), displays group delay with variations less than 1-ns except at the notch frequency band as shown in Figure 7(a).

The antenna transfer function is also calculated and incorporated in Figure 7(b), which is defined as,

$$H(\omega) = \sqrt{\frac{2\pi RcS_{21}e^{j\omega R/c}}{j\omega}} \tag{3}$$

where c is the free-space velocity and R the distance between the two antennas [17]. Fairly flat magnitude variation less than 10 dB is observed in desired frequency band for each port. The input and radiated impulses through port 1 and port 2, given in Figure 8, show that the antenna retains the impulse with minimum dispersion in both cases. Radiated (co-pol) signals are measured using far-field probes placed at $\theta = 0°$ and $\phi = 90°$.

The fidelity factor [F] gives the measure of pulse deformation caused by the antenna. It is required to quantify the signal deformations as the pulses are transmitted or received. It is determined by the

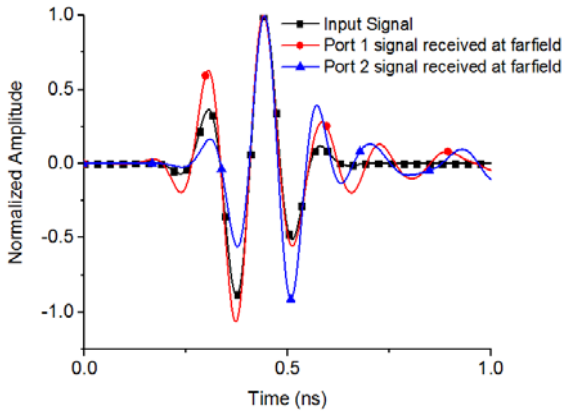

Figure 8. Input and radiated impulses of the antenna.

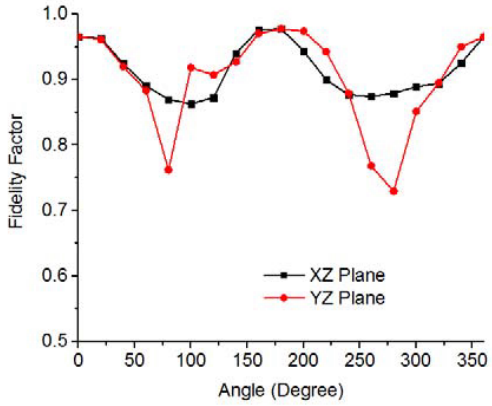

Figure 9. Fidelity factors of the antenna.

absolute maximum of the cross-correlation between transmitted and received time pulses. The Fidelity Factor is defined as [17]

$$F(\theta,\phi) = \max\left[\frac{\int_{-\infty}^{\infty} s_t(t)s_r(t+\tau,\theta,\phi)\,dt}{\sqrt{\int_{-\infty}^{\infty} s_t^2(t)dt \int_{-\infty}^{\infty} s_r^2(t,\theta,\phi)\,dt}}\right] \tag{4}$$

where S_t is the transmitted/input pulse and S_r the measured/received pulse in time domain. It is found that the fidelity factors in various configurations are above 76%, which reveals that the antenna imposes negligible effects on the transmitted pulses. Fidelity factors calculated in both XZ and YZ planes are plotted in Figure 9.

The envelope correlation coefficient (ECC) is an important parameter to evaluate the diversity performance of a MIMO system. It measures the correlation between radiation patterns of the two antenna elements. For a two-port system, the ECC (ρ) can be calculated using Equation (5) proposed in [18] and plotted in Figure 10.

$$\rho = \frac{\left|S_{11}^* S_{12} - S_{21}^* S_{22}\right|^2}{\left(1-\left(|S_{11}|^2+|S_{21}|^2\right)\right)\left(1-\left(|S_{22}|^2+|S_{12}|^2\right)\right)} \tag{5}$$

It is observed that the values of ECC remain low throughout the UWB spectrum except WLAN frequency band, which indicates that the proposed antenna is a good candidate for wireless communication systems with polarization diversity.

The mean effective gain (MEG) is defined as the ratio of the mean received power to the mean incident power of the antenna element. The MEG can be used to quantify the average received signal strength of each antenna element, which can be calculated by the following expression [18]:

$$\mathrm{MEG}_i = \frac{P_{rec}}{P_{inc}} = \oint\left[\frac{\mathrm{XPR}\cdot G_{\theta i}(\Omega) + G_{\phi i}(\Omega)\cdot P_\phi(\Omega)}{1+\mathrm{XPR}}\right]d\Omega \tag{6}$$

In the case of uniform propagation environment where XPR = 1 and $P\theta = P\phi = 1/4\pi$, Equation (6) can be simplified [18]

$$\mathrm{MEG}_i = \frac{e_{Tot}^i}{2} = \frac{e_{mis}^i e_{rad}^i}{2} \tag{7}$$

where, e^i_{Tot} is the total antenna efficiency of the ith antenna element, e^i_{mis} the antenna mismatch efficiency and e^i_{rad} the radiation efficiency which incorporates conduction and dielectric loss. The ratios of mean effective gain are calculated to quantify the power imbalance of the antenna elements. In order to guarantee a good channel characteristic, the signal received from the antennas should satisfy the following criteria [18]

$$\mathrm{MEG}_i/\mathrm{MEG}_j \cong 1 \tag{8}$$

where $i, j = 1, 2, 3$ and 4, which denote the antenna elements 1, 2, 3 and 4, respectively. The proposed MIMO antenna satisfies this criterion which validates that it is a good candidate for MIMO applications. MEGs for the 2 antennas are shown in Figure 11.

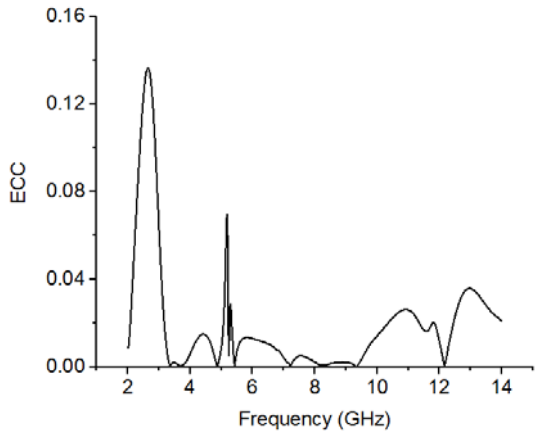

Figure 10. ECC of the proposed antenna.

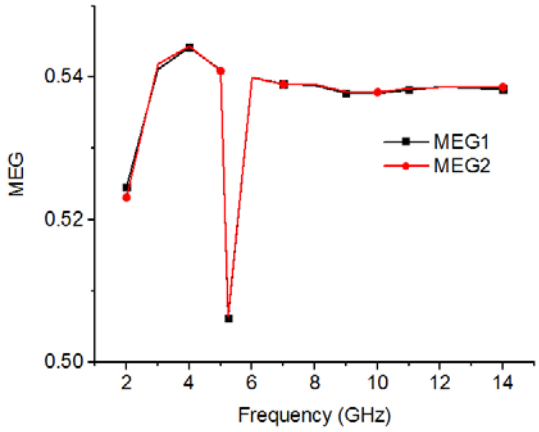

Figure 11. MEGs of proposed antenna.

Diversity gain (DG) is defined as the difference between the selection combined cumulative distribution function (CDF) and one of the other CDFs at certain CDF level, commonly chosen to be 1 percent [4]. The DG of the diversity antenna can be calculated approximately by the formula [19]

$$\mathrm{DG} = \mathrm{DG}_o \cdot \mathrm{DF} \cdot K = \mathrm{DG}_o \cdot \left(\sqrt{1-\rho}\right) \cdot K \tag{9}$$

where DG_0 is the diversity gain of the antenna in the ideal case, ρ the envelope coefficient of the antenna elements, and K the ratio of MEG_i to MEG_j of the antenna element. Figure 12 shows diversity gain of the proposed antenna over the desired frequency band and indicates that the diversity gain of the proposed antenna is pretty good in the UWB spectrum.

3.1. Spatial Domain Analysis

Spatial domain analysis deals with the variation of antenna properties with respect to directions around the antenna. PSF gives a quantitative measure of the variation of radiation pattern with respect to various directions in space as a function of frequency. It is useful as a quantitative measure a) to compare the suitability of different antennas for a given wideband or multiband applications; b) to assess pattern stability improvement methods; and c) to quantify the effect of packaging on stability.

Pattern stability factor [PSF] is an important factor for characterization of wideband antennas. It represents the overall pattern stability of an antenna for a specific bandwidth and range of directions. The PSF [20] of a wideband antenna for a given frequency band can be defined as

$$\mathrm{PSF} = \frac{\int\limits_{\Omega} C\left(\vec{R}\right) ds}{\int\limits_{\Omega} ds} = \frac{\left(\int\limits_{\Omega} F^2\left(\vec{R}, \vec{r}\right) ds \Big/ \int\limits_{\Omega} ds\right)}{\int\limits_{\Omega} ds} \tag{10}$$

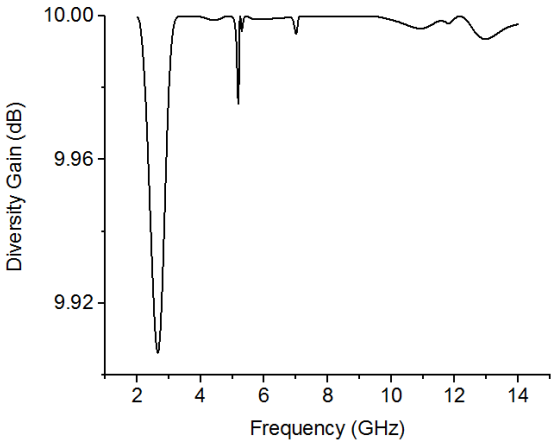

Figure 12. Diversity gain of proposed antenna.

where Ω is the range of operating directions of the antenna; $C(\vec{R})$ is the frequency domain correlation factor, which represents how the radiated waveform in the reference direction $\vec{R}$ is correlated to all other directions $\vec{r}$; $F^2(\vec{R},\vec{r})$ is the frequency domain equivalent of normalized correlation coefficient $f^2(\vec{R},\vec{r})$ in time domain and can be defined as

$$F^2(\vec{R},\vec{r}) = \frac{\left[\int\limits_{\mathrm{BW}} E(\vec{r},f)\, E^*\left(\vec{R},f\right) df\right]^2}{\int\limits_{\mathrm{BW}} \left|E\left(\vec{R},f\right)\right|^2 df \int\limits_{\mathrm{BW}} |E(\vec{r},f)|^2\, df} \tag{11}$$

where, $f^2(\vec{R},\vec{r})$, a quantitative representation of the correlation between reference directions and other directions of interest, is defined as

$$f^2(\vec{R},\vec{r}) = \frac{\left[\int\limits_{-\infty}^{\infty} e(\vec{r},t)\, e\left(\vec{R},t\right) dt\right]^2}{\int\limits_{-\infty}^{\infty} \left|e\left(\vec{R},t\right)\right|^2 dt \int\limits_{-\infty}^{\infty} |e(\vec{r},t)|^2\, dt} \tag{12}$$

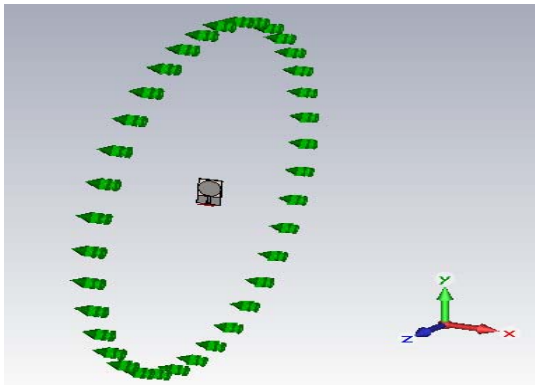

Figure 13. Probe placement for YZ plane E_Φ.

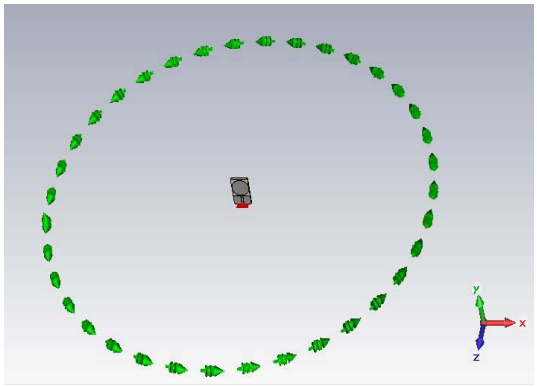

Figure 14. Probe placement for XZ plane E_θ.

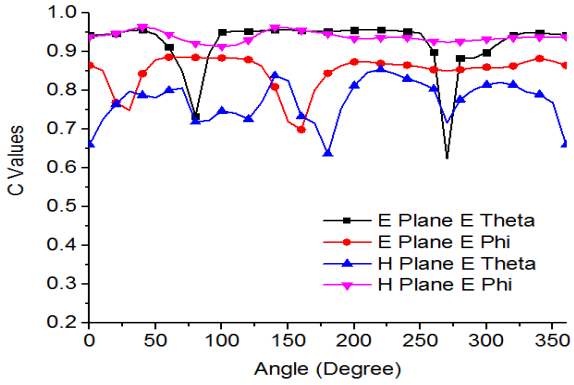

Figure 15. C values of proposed antenna.

Table 2. PSF values of proposed antenna.

Antenna	XZ Plane E_θ	XZ Plane E_Φ	YZ Plane E_θ	YZ Plane E_Φ
UWB-MIMO	0.8498	0.9233	0.9383	0.7767

where $e(\vec{r}, t)$ is the radiated pulse in time domain at a far field point $\vec{r}$, $r = |\vec{r}|$, and $e(\vec{R}, t)$ the reference function corresponding to the radiated field in the reference direction $\vec{R}$. In order to calculate the PSF, the range of directions of interest is discretised, and frequency domain radiated electric field values are detected using virtual probes over the desired directions. The probe orientation and arrangement to calculate PSF for E_θ and E_ϕ components in both XZ and YZ planes are shown in Figure 13 and Figure 14, respectively. Time-domain field pulses $e(\vec{r}, t)$ at 10° interval are obtained using virtual probes in CST. Then FFT of each of these signals, $E(\vec{r}, f)$,is found out. Further C values and PSF calculations are done using MATLAB. Figure 15 shows the calculated C values of the proposed antenna, which result in good pattern stability. It means that the proposed antenna can reach nearly maximum pulse amplitude in all directions independent of the selection of the reference direction. PSF values are given in Table 2.

4. CONCLUSION

In this paper, compact WLAN band-notched floral-shape UWB-MIMO antenna for polarization diversity applications is presented and investigated. Two identical antenna elements in the orthogonal configuration provide polarization diversity. Mutual coupling between the antennas is reduced by placing an isolation stub, which opposes the current flow in the ground plane. To validate the simulated results, an antenna prototype is fabricated and tested. The proposed antenna provides more than 75% antenna efficiency, and its gain varies between 2 dB and 4 dB over the 2.7–10.9 GHz frequency range except 5.1–5.9 GHz WLAN frequency band. It provides omnidirectional pattern, moderate gain, low cross polarization, good pulse handling capability, good pattern stability and good diversity performance in the desired frequency bands, which indicates its suitability for UWB MIMO applications.

REFERENCES

1. "First report and order in the matter of revision of Part 15 of the Commission's rules regarding ultra-wideband transmission systems FCC," ET-Docket 98-153, 2002.
2. Foschini, G. J. and M. J. Gans, "On limits of wireless communications in a fading environment when using multiple antennas," *Wireless Personal Comm.*, No. 6, 311–335, 1998.
3. Dong, L., H. Choo, R. Heath, Jr., and H. Ling, "Simulation of MIMO channel capacity with antenna polarization diversity," *IEEE Trans. Wireless Comm.*, Vol. 4, 1869–1873, 2005.

4. Kildal, P. S. and K. Rosengran, "Correlation and capacity of MIMO systems and coupling, radiation efficiency, diversity gain of their antennas: Simulations and measurements in a reverberation chamber," *IEEE Comm. Mag.*, Vol. 42, No. 12, 102–112, 2004.
5. Ren, J., D. Mi, and Y.-Z. Yin, "Compact ultrawideband MIMO antenna with WLAN/UWB bands coverage," *Progress In Electromagnetics Research C*, Vol. 50, 121–129, 2014.
6. Zhang, S., Z. Ying, J. Xiong, and S. He, "Ultrawideband MIMO/diversity antennas with a tree-like structure to enhance wideband isolation," *IEEE Antennas Wireless Propag. Lett.*, Vol. 8, 1279–1282, 2009.
7. Liu, X. L., Z. Wang, Y.-Z. Yin, and J. H. Wang, "Closely spaced dual band-notched UWB antenna for MIMO applications," *Progress In Electromagnetics Research C*, Vol. 46, 109–116, 2014.
8. Li, Z. Y., Z. W. Du, and K. Gong, "A dual-slot diversity antenna with isolation enhancement using parasitic elements for mobile handsets," *Proc. Asia Pacific Microwave Conf.*, 1821–1824, 2009.
9. Su, S. W., C. T. Lee, and F. S. Chang, "Printed MIMO-antenna system using neutralization-line technique for wireless USB-dongle applications," *IEEE Trans. Antennas Propag.*, Vol. 60, No. 2, 456–463, 2012.
10. Antonino-Daviu, E., M. Gallo, B. B. Clemente, and M. F. Bataller, "Ultra-wideband slot ring antenna for diversity applications," *Electron. Lett.*, Vol. 46, No. 7, 478–480, 2010.
11. Barba, M., "A high-isolation, wideband and dual-linear polarization patch antenna," *IEEE Trans. Antennas Propag.*, Vol. 56, No. 5, 1472–1476, 2008.
12. Li, Y., Z. J. Zhang, W. H. Chen, Z. H. Feng, and M. Iskander, "A dual-polarization slot antenna using a compact CPW feeding structure," *IEEE Antennas Wireless Propag. Lett.*, Vol. 9, 191–194, 2010.
13. Ojaroudi, M., S. Yazdanifard, N. Ojaroudi, and R. A. Sadeghzadeh, "Band-notched small square-ring antenna with a pair of T-shaped strips protruded inside the square ring for UWB applications," *IEEE Antennas Wireless Propag. Lett.*, Vol. 10, 227–230, 2011.
14. Yazdi, M. and N. Komjani, "Design of a band-notched UWB monopole antenna by means of an EBG structure," *IEEE Antennas Wireless Propag. Lett.*, Vol. 10, 170–173, 2011.
15. Jiang, W. and W. Q. Che, "A novel UWB antenna with dual notched bands for WiMAX and WLAN applications," *IEEE Antennas Wireless Propag. Lett.*, Vol. 11, 293–296, 2012.
16. Zhao, J.-Y., Z.-Y. Zhang, Q.-Q. Liu, G. Fu, and S.-X. Gong, "Printed UWB MIMO antenna with different polarizations and band-notch characteristics," *Progress In Electromagnetics Research Letters*, Vol. 46, 113–118, 2014.
17. Sharma, M., A. Alomainy, and C. Parini, "Fidelity pattern analysis of a CPW feed miniature UWB antenna using diff. Excitation pulses," *IEEE Antennas Wireless Propag. Lett.*, Vol. 14, 494–498, 2015.
18. Karaboikis, M. P., V. C. Papamichael, G. F. Tsachtsiris, and V. T. Makios, "Integrating compact printed antennas onto small diversity MIMO terminals," *IEEE Trans. Antennas Propag.*, Vol. 56, No. 7, 2067–2078, 2008.
19. Gao, Y., X. D. Chen, and Z. N. Ying, "Design and performance investigation of a dual-element PIFA array at 2.5 GHz for MIMO terminal," *IEEE Trans. Antennas Propag.*, Vol. 55, No. 12, 3433–3441, 2007.
20. Dissanayake, T. and K. P. Esselle, "Correlation based pattern stability analysis and a figure of merit for UWB antennas," *IEEE Trans. Antennas Propag.*, Vol. 52, No. 11, 3184–3191, 2006.